

# Electron irradiation induced reduction of the permittivity in chalcogenide glass ( $\text{As}_2\text{S}_3$ ) thin film

Damián P. San-Román-Alerigi,<sup>1</sup> Dalaver H. Anjum,<sup>2</sup> Yaping Zhang,<sup>1</sup> Xiaoming Yang,<sup>2</sup>

Ahmed Benslimane,<sup>1</sup> Tien K. Ng,<sup>1</sup> Mohammad Alsunaidi,<sup>1,3</sup> and Boon S. Ooi<sup>1</sup>

<sup>1</sup>*Photonics Laboratory, King Abdullah University of Science and Technology (KAUST), Thuwal 21534, Saudi Arabia\**

<sup>2</sup>*Advanced Nanofabrication and Imaging Core-Lab, King Abdullah University of Science and Technology (KAUST), Thuwal 21534, Saudi Arabia*

<sup>3</sup>*King Fahd University of Petroleum and Minerals (KFUPM), Dhahran 31261, Saudi Arabia*

## Abstract

*In this paper we investigate the effect of electron beam irradiation on the dielectric properties of  $\text{As}_2\text{S}_3$  Chalcogenide glass. By means of low-loss Electron Energy Loss Spectroscopy, we derive the permittivity function, its dispersive relation, and calculate the refractive index and absorption coefficients under the constant permeability approximation. The measured and calculated results show, to the best of our knowledge, a heretofore unseen phenomenon: the reduction in the permittivity of  $\geq 40\%$ , and consequently a modification of the refractive index follows, reducing it by  $20\%$ , hence suggesting a significant change on the optical properties of the material. The plausible physical phenomena leading to these observations are discussed in terms of the homopolar and heteropolar bond dynamics under high energy absorption. The novel phenomena exhibited by  $\text{As}_2\text{S}_3$ -thin film can be capital for the development of photonics integrated circuits using electron beam irradiation method.*

Keywords:  $\text{As}_2\text{S}_3$ ; chalcogenide glasses; permittivity; dielectric properties; electron irradiation; Electron Energy Loss Spectroscopy.

---

\* email: damian.sanroman@kaust.edu.sa

## I. INTRODUCTION

Over the course of the last decades chalcogenide glasses have been a subject of great interest due to the myriad photon-induced phenomena they exhibit, enthralling the imagination of scientists and engineers to prompt a sundry of photonic applications relevant to countless areas of research and engineering, ranging from biology[1, 2] and telecommunications[3, 4], all-optical chips [2, 4], single photon sources [5, 6] and holography[7]. Still and all, as fascinating the applications from chalcogenide glass may be, they have withal been worthy of great attention from fundamental sciences, owing to the seemingly oxymoronic nature of the physical effects observed in multiple experiments, *e.g.* giant photo-expansion[8] *versus* photo-contraction[9], photo-liquidity[10, 11] *versus* photo-crystallization[12, 13], photo-darkening[14, 15] *versus* photo-bleaching[14], and namely photo-refraction[15–18], to name a few; all taking place upon illumination with light within a comparable energy range to that of their band-gap,  $E_g \sim 2.4\text{eV}$ . Studies from fundamental physics and material science have led to various models to explain the mechanisms behind the exciting structural reconfiguration capabilities and phenomena observed in them upon energy absorption. That being said, the physical processes, as well as many of the phenomena reported, still remain both a matter of debate and a hot topic in fundamental and applied research.

The principal experiments, observations and models in chalcogenide glass deal with phenomena triggered by light irradiation. Photon induced phenomena in chalcogenide glass comprise: *photon-induced*-refractive index modification, -liquidity, -dichroism, -anisotropy, -crystallization, -darkening, -bleaching, and -vitrification [8–19], in addition to other innate effects present in highly non-linear materials, *v.gr.* second harmonic generation [20, 21]. To understand the nature of these effects, and the electronic and atomic processes involved, it is essential to investigate the charge carrier transfer, energy spectrum, and the mechanism of radiation (electron or photon) interaction with the material and its chemical and atomic structure [9, 11, 13, 22–26].

Electron irradiation induced refractive index modification has also been observed. Suhara *et al.*[27], found a maximum change of  $\Delta n/n = +3.6\%$ , with no significant modification of the film's thickness. Alternatively, Normand *et al.*[28–30] and Tanaka *et al.*[31], inde-

pendently, have observed a  $\sim 3\%$  increment in the refractive index of chalcogenide glass; concurrent to the formation of trenches and mounds, 180 nm and 110 nm respectively, in chalcogenide films 5 – 11  $\mu\text{m}$  thick. They posited that the morphological and optical alteration derived from the structural reorganization and re-bonding of the homopolar and heteropolar bonds, in addition to the electrostatic effects arising from the charge density variation [28–31].

Whilst many of these effects allure our research interest, we are particularly intrigued by the alteration in the optical properties of chalcogenide thin films, and their possible myriad applications. However, in most of the previous studies concerning this subject, only the refractive index has been measured, and little information is available on how the electromagnetic components, *permittivity* and *permeability*, reshape under energy absorption. In this paper we present the results of our investigation on the permittivity of chalcogenide  $\text{As}_2\text{S}_3$  thin film by means of low-loss electron energy loss spectroscopy (EELS); and its dynamics upon energy absorption. We believe that understanding the electromagnetic characteristics and their dynamics, particular to this material, are key to enable and extend many of the devices proposed by transformation optics and achieve light control beyond the scope of [meta]materials.

We have organized the paper in the following fashion, section I presented a review on the subject at hand. In section II, we introduce the theoretical and experimental methodology needed to explain the experimental results. Section III presents the results and analysis, followed by the deduction of the refractive index under the constant permeability approximation, while discussing its implications. Finally, in section IV, we present our conclusions.

## II. METHODS

It is worth to discern the difference, and connection, between the refractive index and the electromagnetic properties of materials. The former is the ratio between the propagation speed of waves inside a material to that of vacuum; whereas the latter, permittivity ( $\epsilon$ ) and permeability ( $\mu$ ), are the physical representation of a material's intrinsic electric and

magnetic properties; which arise from the atomic, electronic and molecular configuration and interactions with the electric and magnetic fields, ultimately shaping their propagation dynamics. Accordingly, the refractive index and the electromagnetic properties of materials are entwined by the widespread relation:  $n = \sqrt{\varepsilon_r \mu_r}$ , where the subscript  $r$  refers to the relative permittivity or permeability, *i.e.*  $\varepsilon_r = \varepsilon/\varepsilon_0$  and  $\mu_r = \mu/\mu_0$ .

Permeability and permittivity are, then, key to manipulate light propagation in materials, and hence the importance of characterizing them, and understanding how can they be modified.

### A. Electron Energy Loss Spectroscopy

As discussed earlier,  $\text{As}_2\text{S}_3$  chalcogenide glass, exhibits electron- and photon- irradiation induced modification of its optical properties. In our study we use low-loss EELS[32, 33] to characterize the real and imaginary parts of the permittivity of  $\text{As}_2\text{S}_3$ .

In our EELS experiment, the material is exposed to an electron beam setup *a priori*, with energy,  $E_e$ , usually in the order of  $10^3$  eV. If the sample is sufficiently thin,  $\leq 500\text{nm}$ , a vast majority of the electrons will pass through the sample without being perturbed, but a small fraction of them will undergo inelastic scattering loosing energy to the sample, typically in the order of  $10^3$  eV. It is important to note that while some elastically scattered electrons will also transfer some energy to the system, this is not enough to perturb the overall atomic arrangement of the sample. Even on a head-on collision with the atom the elastic scattered electron energy loss will be in the range of 1 eV, which is not sufficient to displace the atoms and thus change the molecular arrangement. The inelastic scattering however yields enough energy to the system to sustain bond-breaking and alterations in the electron density. The latter electron loss can be experimentally measured via an electron spectrometer.

The inelastic scattering process is characterized by the scattering angle  $\theta$ , or the momenta  $\vec{q}$ , and the energy loss  $E_s$  due to their interactions with the material, which include phonon excitation, inter- and intra- band transition, plasmons excitation, inner shell ionization,

and Cherenkov radiation. These interactions can be summarized by the dielectric response function,  $\varepsilon(\vec{q}, \omega)$ ; which describes the interaction of photons and electrons with the material [33].

Admittedly, the interaction of photons and electrons with those in the solid is different; photons displace the electrons in the material in a direction perpendicular to their direction of propagation, with the electron density remaining unchanged, therefore we define the *optical permittivity* as a transverse property of a medium; whereas electrons interacting with the material produce a longitudinal displacement of the electrons, and change the electron density. Moreover, the energy transfer mechanisms for photons differs from that of electrons; in the former the energy transfer is mostly mediated by inter- and intra- band transitions (valence-to-conduction band), *e.g.* (i) bandgap absorption, (ii) defects, (iii) free carriers, among other transitions. In the scenario of electron irradiation, energy transfer takes place by means of inelastic scattering, and to a lesser degree by elastic scattering. Despite the fundamental differences, however, it is possible to establish a correlation between the permittivity measured by electrons or photons if we constrain to small energy losses, which translates small scattering angles for electrons. Under this condition  $\varepsilon(\vec{q}, \omega)$  varies insignificantly with  $\vec{q}$ , and hence  $\varepsilon(\vec{q}, \omega) \approx \varepsilon(\vec{q} = 0, \omega = E/\hbar)$ , the latter being the optical permittivity [33–35].

Whence stems the versatility of low-loss EELS over other methods to measure the permittivity of thin film samples constraint to small probing areas. Specifically, if scanning transmission microscopy (STEM) is used, the volume of study can be reduced to nanometric scale, allowing us to study the material and its response locally. As discussed in the preceding paragraph, in a typical EELS experiment low angles of collections are used, and thus most inelastic collisions result in energy losses to the incoming electrons of less than 100 eV. This energy loss range in turn deciphers information about the permittivity within an energy range of interest to optics and photonics, *i.e.*  $\leq 10$  eV. The latter is achieved by post-processing the energy loss spectra by means of Kramers-Kronig relations to evince the real and imaginary parts of the optical permittivity [33, 36–41].

## B. Experimental arrangement

In our experiment, high energy electrons (  $300\text{ keV}$ ) impinge on an  $\text{As}_2\text{S}_3$  thin film,  $300\text{ nm} \pm 5\text{ nm}$  thick, grown on a  $2\text{ }\mu\text{m}$  holey-Cu TEM grid by means of electron-beam evaporation, and the roughness, film thickness and stoichiometry are characterized by *atomic force microscopy ellipsometry*, and EDX.

To ensure the validity of the low energy loss limit approximation, we use a scanning transmission electron microscope (STEM), coupled to a low-loss EELS and perform the experiment in the low momentum transfer relativistic approximation. We set the electron source to  $300\text{ keV}$ , with a collection angle of  $6\text{ mrad}$ , and incident semi-angle of  $4.575\text{ mrad}$ . Under these conditions the energy resolving power of the electron loss spectrometer is better than  $0.1\text{ eV}$  in the range  $0.8\text{ eV} - 50\text{ eV}$ ; electrons are accelerated to  $77.561\%$  the speed of light, corresponding to a de Broglie wavelength of  $1.9687 \times 10^{-3}\text{ nm}$ , which results in a minimum spatial resolution of  $1.2048 \times 10^{-1}\text{ nm}$ . The scanning area for the STEM is  $50 \times 50\text{ nm}$  square on the holey region of the film support, to avoid any contamination from the carbon support of the grid. The density of electrons per second incident on the sample is  $175\text{ e}^-/\text{nm}^2\text{s}$ . To achieve different electron dosages we control the irradiation time in steps of  $1\text{ ms}$  (see table I). Additionally, irradiation is done in two slots, namely set *A* and set *B*; separated by a relaxation zone defined as the time where zero electrons are incident on the sample. These three regimes allow us to determine if, after a given time of repose, the material returns to its initial state, i.e. if it shows memory or a hysteretic behaviour.

Sample	1	2	3	4	Relax	5	6
Exposure time $t^*$ (s)	0.1	0.2	0.3	0.5	60	0.8	1.0
Accumulated time $t$ (s)	0.1	0.3	0.6	1.1	-	0.8 + 1.1	1.8 + 1.1

TABLE I: Experimental irradiation time and dosage. The symbol “+” is used to demark that the material was subject to irradiation for a given time before the new measurement.

### III. OBSERVATIONS AND ANALYSIS

As discussed earlier in the text, we study the energy loss spectra of transmitted electrons in the low momentum transfer relativistic approximation, customarily known as low-loss EELS. The experiment results is a spectra-like graph detailing the density of electrons versus their output energy, at different irradiation dosages.

#### A. Results analysis

In order to obtain the optical and electronic characteristics of the material, the loss spectra needs to be deconvoluted, and the zero loss subtracted: this is attained by the Fourier-Log Two Gaussian method [33] (see figure 1).

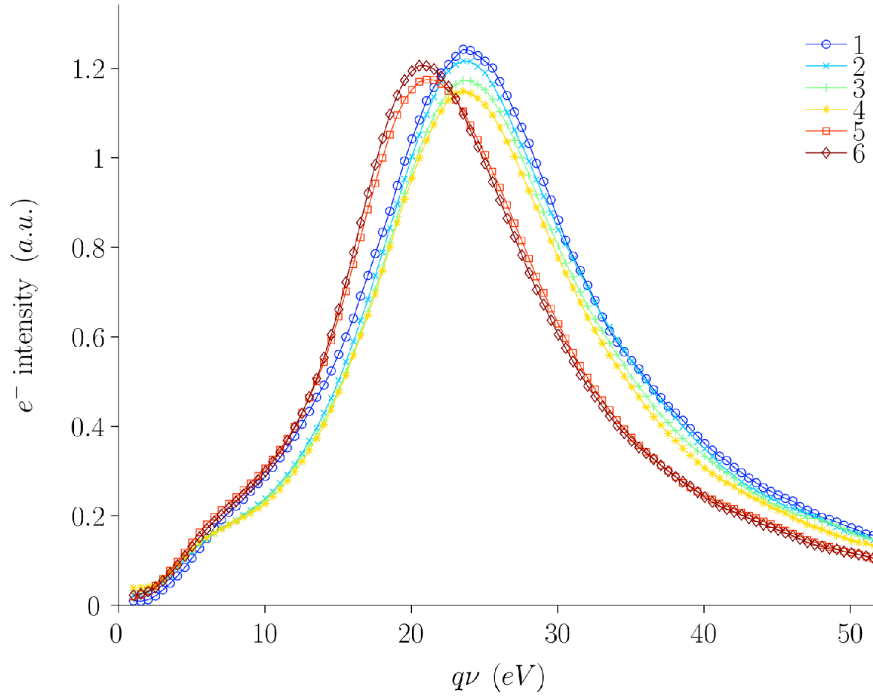


FIG. 1: Low-loss Electron Energy Loss spectra, raw measurement results at different dosages as specified in table I. The causal variable marks the energy lost by the electrons to the material through inelastic scattering.

A meticulous inspection of figure 1 reveals that the peak of the loss spectra decreases

as a function of dosage as depicted in figure 2b), after four dosages, and before relaxation, the peak value changes 8%. It is also evident that the process has some degree of elasticity, where after relaxation some recovery of occurs such that the electron intensity before and after relaxation suffers a 2% return (see figure 2b), however this return goes hand in hand with a blue-shift of the peak dispersion of  $\sim 3$  eV . Yet there is a striking effect subsequent irradiation for long periods of time has a reverse effect increasing the total electron intensity, rather than decreasing it as was the case before relaxation. As we will elucidate later this effect can be explained by the breaking of the homopolar bonds, and the continuous reconfiguration of the heteropolar bonds within the material. Is capital to recall that our experiment is carried in a vacuum environment ( $10^{-8}$  Torr), therefore eliminating any chance of oxidation and contamination on the material surface.

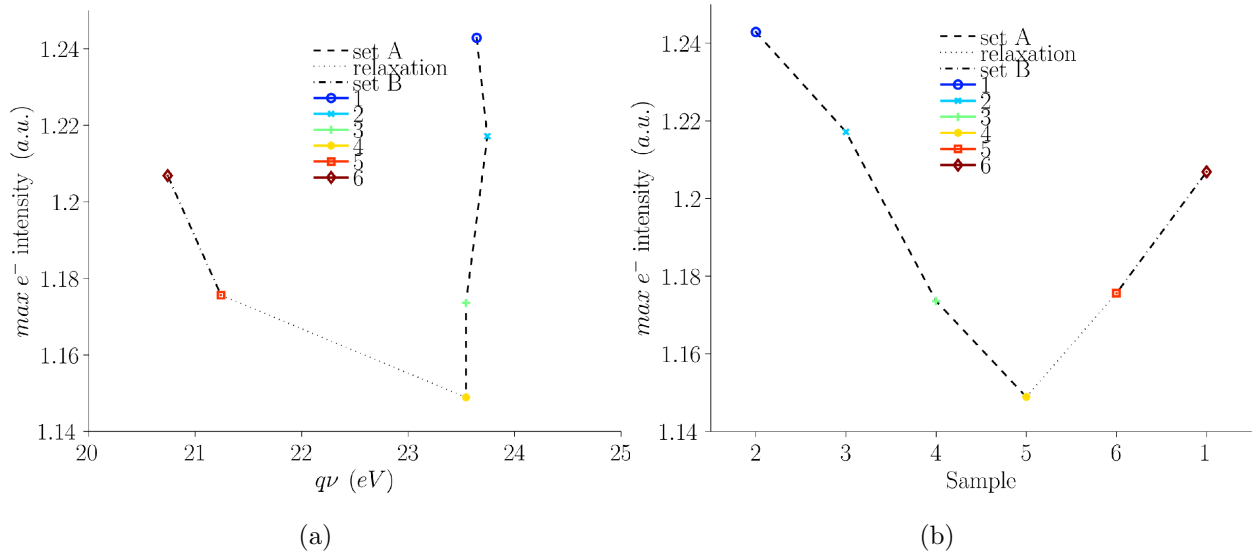


FIG. 2: Analysis of peak loss for samples 1 through 6, the peak position versus energy loss  $q\nu$  is shown in (a); while the behaviour of the peak in reference to sample, or dosage, is plotted in (b).

As discussed earlier, the electron energy loss is linked to the real and imaginary permittivity (see equation 1), and hence we can expect them to follow a somewhat similar pattern to that of the energy loss. [33].



$$\sigma_{eels} = \Im(-1/\varepsilon) = \frac{\varepsilon_2}{\sqrt{\varepsilon_1^2 + \varepsilon_2^2}}. \quad (1)$$

By virtue of the above equation and the Kramers-Kronig relations we obtain the *imaginary* part of the permittivity function,  $\varepsilon_2 = \Im(\varepsilon)$ , and the *real* part,  $\varepsilon_1 = \Re(\varepsilon)$ , here shown in figure 3.

It is essential for the ongoing discussion to remark that in the curves of figure 3, and subsequent, the causal variable,  $h\nu$ , refers to the photon energy, for recall that these result from the Kramer-Kronig analysis on the electron energy loss spectra at the low momentum approximation. Therefore, they can be regarded as dispersion relations for the permittivity at different irradiation dosages.

As predicted at analyzing the electron energy loss spectra, the real and imaginary parts of the permittivity decrease as the electron dosage augments. Moreover, figures 3c and 3d confirm the hysteretic comportment of the permittivity. Particularly, observe that the maxima of  $\varepsilon_1$  reduces, and shifts following a hysteresis loop, as the total dosage rises; while its minima shifts to higher energies, although seldom changing its dispersion energy  $h\nu$ . On the other hand, the maxima of  $\varepsilon_2$  exhibits a similar decrement, as that portrayed by  $\varepsilon_1$  as a function of dosage, with the difference that there is no evidence of a hysteretic behaviour, rather the maximum shifts to higher energies together with electron dosage.

To acquire a deeper insight on the material's permittivity dynamics we sample it by splitting the dispersion energy range into two sets, *range A* comprises energy values around the *bandgap* of the material,  $2.0\text{eV} \leq h\nu \leq 3.6\text{eV}$ ; and *range B* includes higher energies  $4\text{eV} \leq h\nu \leq 10\text{eV}$ . Within *Range A* the sampling results compiled in figures 4a and 4c clearly evince the hysteretic behaviour of the electron-induced permittivity change. At comparing the curves given by the maximum peaks of  $\varepsilon_1$  and  $\varepsilon_2$ , before and after relaxation, it is patent that some degree of restoration occurs in the system which allows a recovery of up to 75% of the initial values. Furthermore, the dynamics of the extreme values of either the real or imaginary permittivity echo an almost identical pattern, with an initial fast rate of change at the first irradiation steps  $0 \leq t^* \leq 0.2$  ms, closely followed by a sustained decrement

on its absolute value, *i.e.* the pace at which the permittivity changes tends to zero for a sufficiently large irradiation time (see figures 5). As we will explain in section III B this effect can be explained by the variation in the density and rearrangement of the homopolar and heteropolar bonds, which significantly modifies the material's response to energy absorption.

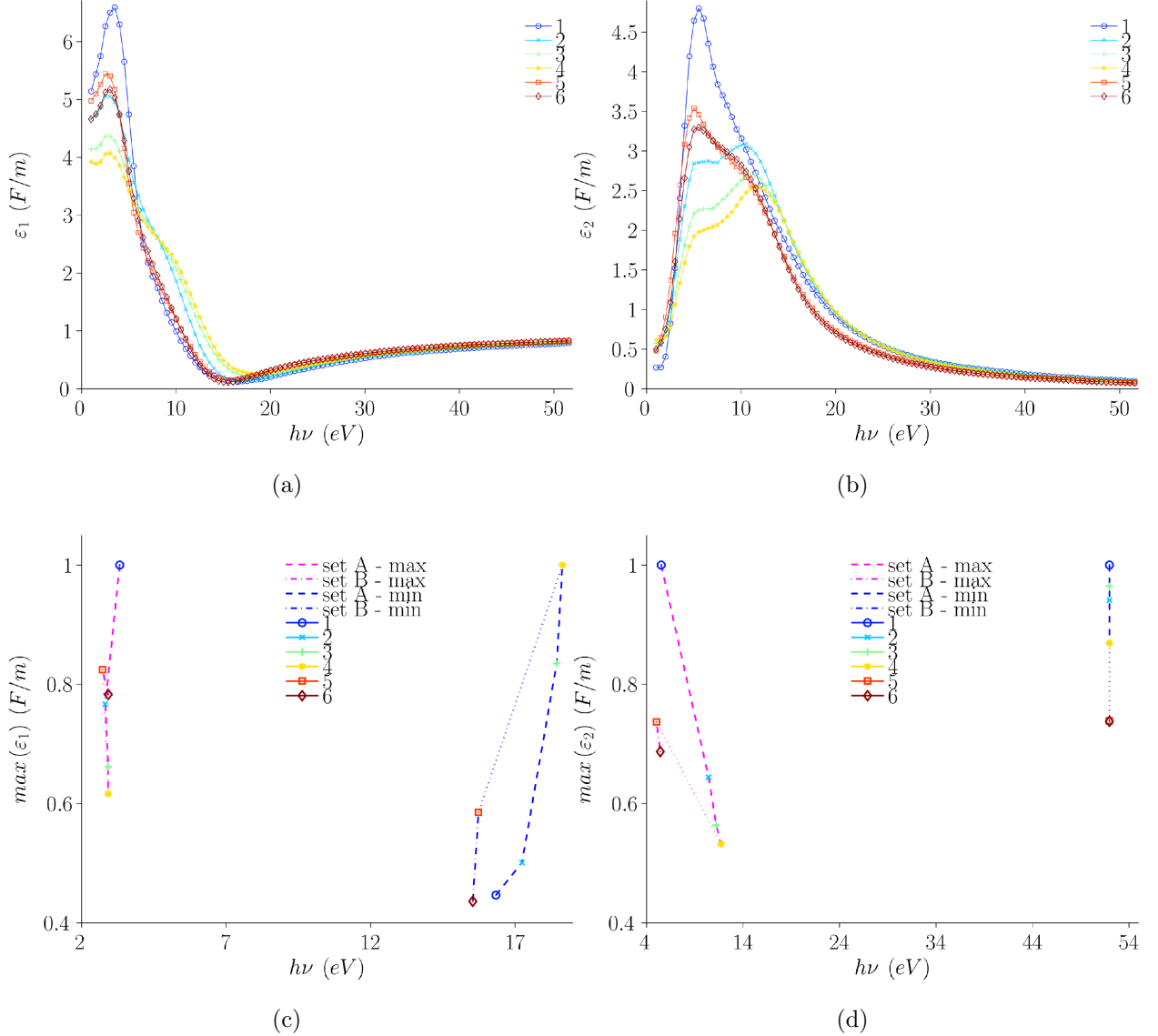


FIG. 3: (a) Real ( $\varepsilon_1$ ) and (b) imaginary ( $\varepsilon_2$ ) parts of the transversal permittivity function derived via Kramers-Kronig relations from the electron energy loss spectra. The peak trace, *i.e.* dispersion relations, for (c)  $\varepsilon_1$ , and (d)  $\varepsilon_2$ , clearly show the heterocitic behavior of the permittivity.

As it can be appreciated at comparing the results between the two energy ranges, either for real or imaginary parts of the permittivity, shows significantly different comportments. The test values for the real permittivity in *range A* closely follow the pattern and magnitude modification of the global maximum, while the global minimum remains virtually unperturbed. In *range B*, however, the selected values present different bearing to that observed in the previously. Specifically, before relaxation samples at  $h\nu \geq 6$  eV initially increase in magnitude as much as 10%, in contrast to the marked decrease of the global maximum.

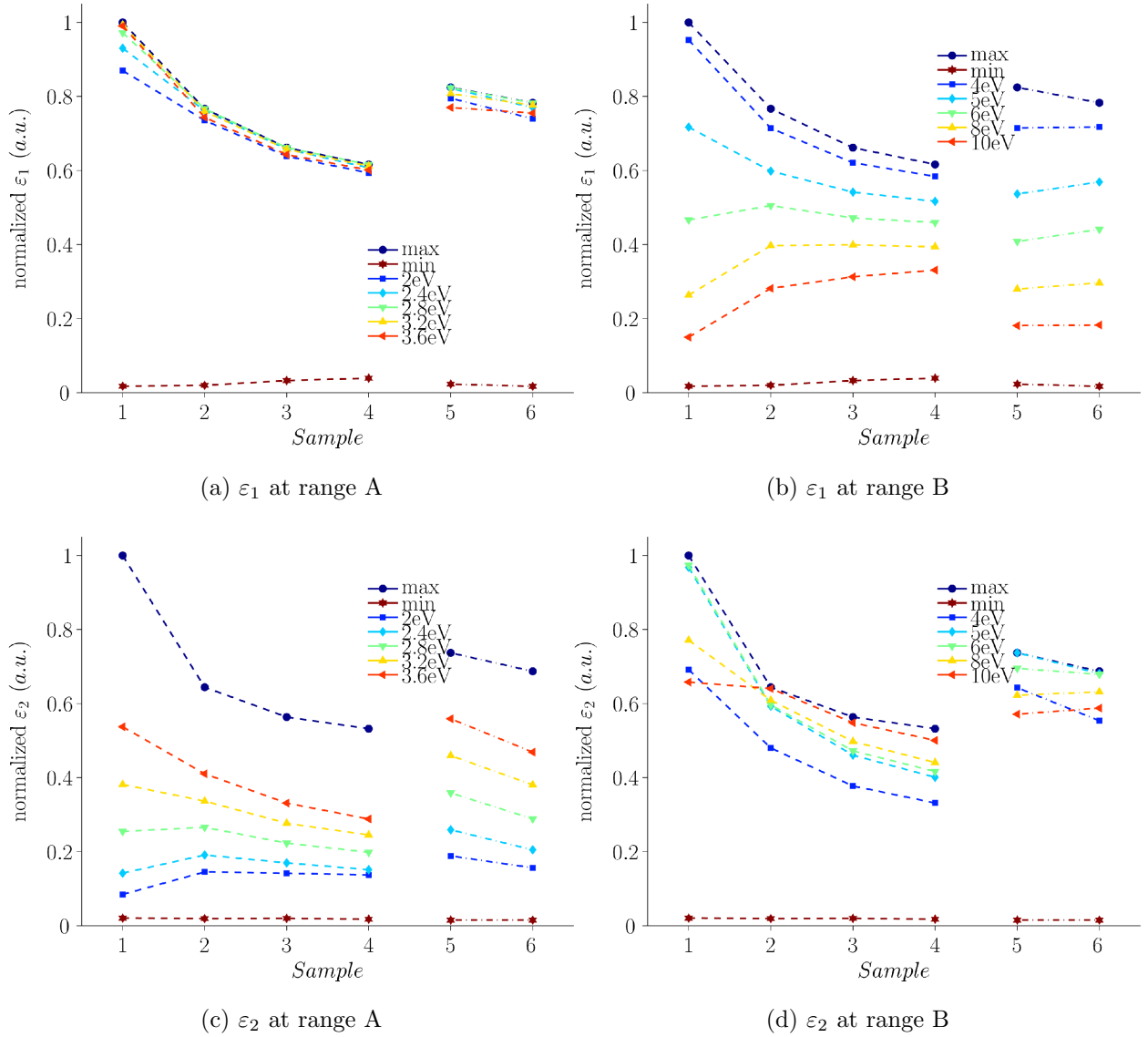


FIG. 4: Selected samples of the permittivity function  $\epsilon$  (real and imaginary) in reference to the dispersion energy, *range A* (a) and (c), and *range B* (b) and (d), at different irradiation dosages.

Yet, with the exception of the sample at 10 eV subsequent electron exposures regain the decreasing pattern of the maximum, albeit to a lesser magnitude, and rate of change (see figure 5b). After relaxation, however, some degree of elasticity is observed, with most of the test samples recovering to the initial state, although exposing the relaxed material anew to electron irradiation results in an increment of the permittivity value in clear contrast to the global maximum bearing.

Concerning the imaginary part of the permittivity, the previous description gets somewhat inverted when compared to the measurements of  $\varepsilon_1$  in both ranges. In *range A* the initial behaviour is mixed, with some of the samples increasing in magnitude, while others decrease. Notably, test samples below the band-gap energy of the material show a similar behavior to that of the imaginary permittivity in *range A*, an initial increment followed by a steady decrease with new dosages. *Range B* on the other hand shows a behavior close to the comportment of the global maximum, with the anomaly of test sample at 10 eV. After relaxation the degree of recovery is mixed, in *range B* the hysteretic behaviour is conspicuous. But in *range A* the results are to some extent extraordinary, all the samples beyond the band-gap of the material show some degree of recovery, in some cases surpassing the initial value by as much as 15% for example at 3.6 eV; below the band-gap energy test samples show an eerie result not only there is no recovery to the initial state, but a considerable increment instead. After relaxation all samples show the same decreasing pattern as observed in their real counterpart. In *range B* all the samples follow a similar pattern to that of the maximum; an initial fast decrease, followed by a sustained decrease in magnitude, although steadily reducing the rate of change. The physical explanation to this curious reaction of the material, reflected by the permittivity, in response to electron bombardment can be reasoned in term of the modification to the physical bonding between the Arsenic and Sulfide atoms, and the electron traps within the material, assuming that there is no increment in the initial number of electrons in the material, which to this effect is grounded.

## B. Physical process

To fathom the physical process behind this phenomenon it is necessary to gain some understanding about the atomic configuration of  $\text{As}_2\text{S}_3$  chalcogenide glass. Either amorphous or crystalline, the structure of chalcogenide material based on As and S is composed of pyramidal arrangement in threads that form layers linked by homopolar (As–As and S–S) and heteropolar (As–S) bonds (figure 6). The bonding energies in the homopolar case are 1.88 eV and 2.39 eV for As–As and S–S bonds, respectively; whilst for the heteropolar

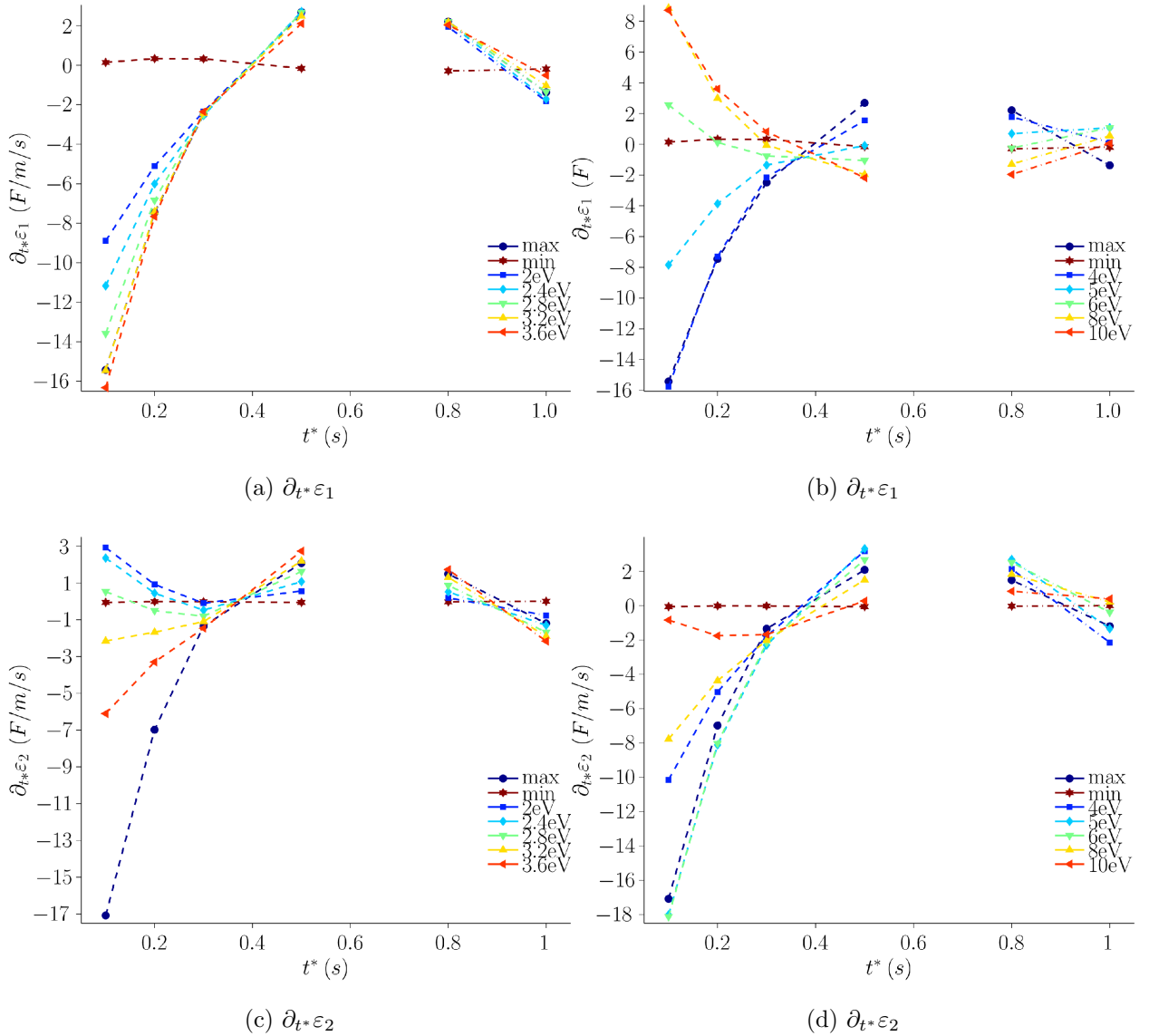


FIG. 5: Derivatives of the permittivity function with respect to the causal variable dosage,  $t^*$ .

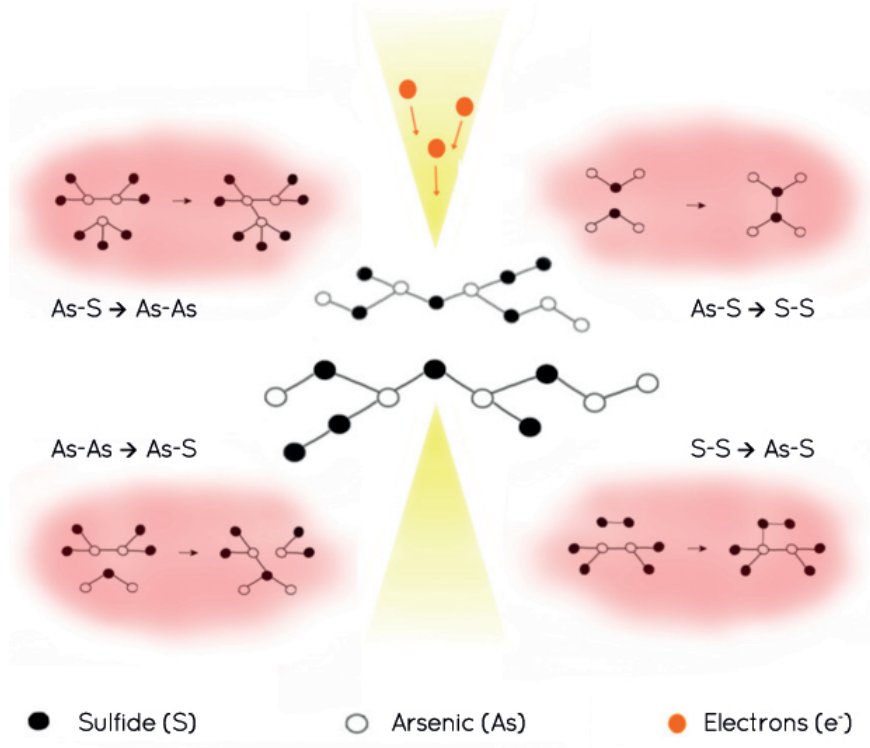


FIG. 6: Homopolar and heteropolar bond breaking process under electron irradiation in  $\text{As}_2\text{S}_3$ .

(As-S) the bonding energy is 2.29 eV [42]. Our sample has a similar proportion of As and S atoms, 51% and 49% respectively, as measured by XPS. The atomic composition measured before and after the experiment did not show any net flux of atom concentration. The incoming electrons (300 keV) can break the homopolar and heteropolar bonds with ease by mean of inelastic collisions; whence a structural rearrangement follows, with the broken homopolar bonds switching to heteropolar bonds [43, 44]. This structural rearrangement will continue for as long as the material keeps being bombarded with electrons. However, since the concentration of As atoms is higher, the re-bonding of the S and As atoms, mostly coming from the broken homopolar bonds, will lead to dangling uncoordinated As atoms. Under relaxation, the dangling As atoms, in vacuum, re-bond in homopolar As-As pairs. Consequently, the density of homopolar bonded As increases, resulting in a diminished response to electron irradiation as observed in the decrement in the rates of change before and after the first irradiation and relaxation period 5.

Concomitant to the re-bonding process is the nano-crystallization of the material, which causes a reduction in the number of the trapped carriers, either by promoting a large fraction

of the electrons to the conduction band, or by reducing the number of carrier traps in the material. The overall modification of the electronic density states originates the prominent reduction in the permittivity. Recall that in amorphous and semi-crystalline materials the permittivity heavily depends on the density of trapped carriers. This comes from the fact that carrier transport in these materials, like chalcogenide glass, is controlled by traps; at any given point in time a fraction of the carriers is confined, and since the dipole moment of the filled and empty traps may vary broadly it changes the permittivity of the material [25, 45]. A working model for the dielectric constant based on the electron trapping was given by Arkhipov *et al.*[46],

$$\varepsilon(\vec{r}, t) = \varepsilon_0 + 4\pi\kappa_0 \int_0^\infty \rho(\vec{r}, t; E)dE, \quad (2)$$

where  $\rho dE$  is the carrier density trapped in the energy interval  $E$  to  $E + dE$ ,  $\vec{r}$  is the position vector,  $t$  the time,  $E$  is the trap energy,  $\varepsilon_0$  is the vacuum permittivity, and  $\kappa_0$  is a coefficient that depicts the change in the dipole moment of the traps due to the capturing of electrons in them. Observe that in order to reduce the permittivity at  $t > t_0$  a reduction in the density of trapped electrons is inexorable, *i.e.*  $\rho(\vec{r}, t, ; E) < \rho(\vec{r}, t_0, ; E)$ .

Evidence of such electronic rearrangement under energy absorption by  $\text{As}_2\text{S}_3$  chalcogenide thin film has been reported separately by Tanaka *et al.* and Lee *et al.*. Tanaka *et al.* [47], observed chemical and medium range re-ordering in  $\text{As}_2\text{S}_3$  film under photon energy absorption. Meanwhile, using X-rays, Lee *et al.* observed modification in the structure order of chalcogenide films [48]. Albeit focusing on the dynamics of photo-darkening and anisotropy, respectively, both studies show that upon energy absorption the material suffers an alteration in both the electron energy density and the bond structure; in agreement with our observations, where the alteration of the permittivity springs from the changes in the structural and electronic states of the film.

### C. Prospective deduction, the refractive index

Earlier we discussed the inextricable relation between the refractive index  $n$  and absorption  $k$ , with the electromagnetic properties of the material,  $\varepsilon_r$  and  $\mu_r$ . Often, in the deduction of the refractive index, the permeability  $\mu_r$  is set to a constant value, generally 1. Resulting in a set of relations widely available in the basic literature. Here we present the calculated optical parameters  $n$  and  $k$  based on them (see figure 7).

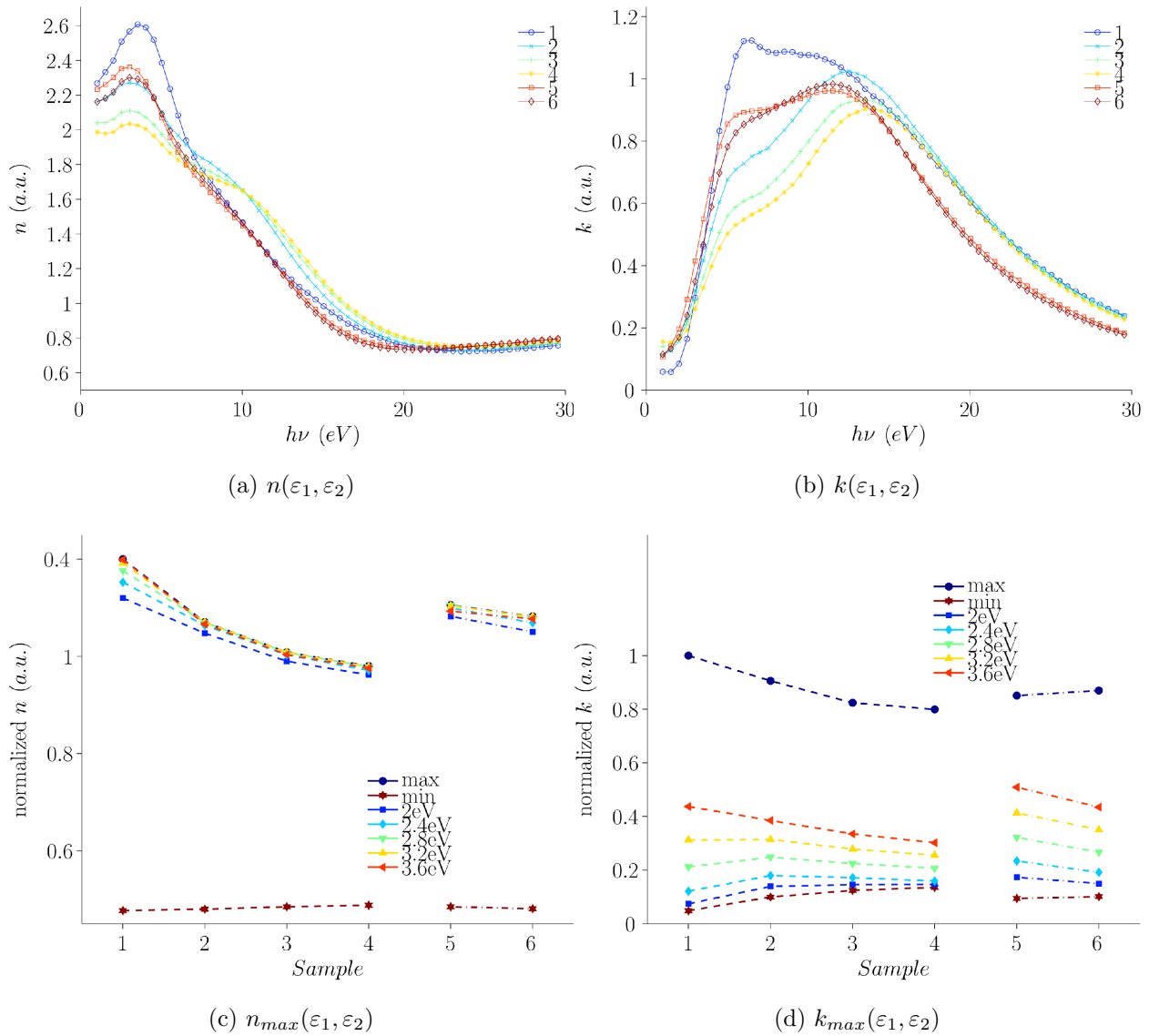


FIG. 7: (a) Refractive index  $n$ , and (b) absorption constant  $k$ , derived from the real and imaginary permittivity. The trace at peak values and sampling at different dispersion energies.



Under the former assumption, the computed results show a similar behaviour for  $n$  and  $k$  to those observed for  $\varepsilon_1$  and  $\varepsilon_2$ , with the refractive index  $n$  peak reducing  $\sim 23\%$  after an irradiation time of  $t = 1$ . The minimum change takes place at 6.5 eV where the reduction is  $\sim 8\%$ . For energies close to the band-gap the reduction is on average approximately 20%. The absorption  $k$  also shows a striking decay down to 40% for its peak value, and a minimum of  $\sim 10\%$ , with an average reduction of  $\sim 35\%$  for dispersion energies close to the band-gap. Calculation of the extrema of the refractive index and absorption coefficient are shown in figures 7c and 7d.

The observed measurements, and the calculated optical properties therein, are extraordinary, in the sense that all previously published experiments, with high energy electrons (40 keV), reported an increase in the refractive index between 3% to 8% [27–31, 49]. In addition to the vast literature reporting photon-induced refractive index change, which has yielded as much as an 8% increase in the refractive index of  $\text{As}_2\text{S}_3$  film under illumination [13, 15]. Yet, under the constant permeability approximation, in our experiment the refractive index decreases as much as 23%. Bearing in mind that the conditions in the cited experiments are significantly different from those here reported, we believe the discrepancy could be explained by two different mechanisms. The first would state that, as described in the previous section, the permeability remains unchanged, while the number of electrons increases, the number of homopolar and heteropolar bonds broken does as well, leading to the recombination mechanism described earlier. These structural alterations in turn induce nano-crystallization, ultimately leading to the generalized reduction on the number of energy traps, especially within energies within *range A*; altogether will cause the reduction in the permittivity, and therefore reduce the refractive index.

On the other hand, to bring to terms the previous published results and ours, it would be necessary for acknowledge a dynamical change of the permeability, with respect to electron irradiation. This would require the electrons to alter the atoms intrinsically by means of elastic collisions, and/or induce current loops, causing the magnetic dipoles in the material to reorganize, *i.e.* inducing paramagnetic states, and hence increasing the permeability. However plausible the latter explanation could be, an experimental confirmation is required, together with further studies on the permeability of Chalcogenide glass under high energy

electron- and photon- irradiation.

#### IV. CONCLUSIONS

A new characterization procedure and analysis of the permittivity of  $\text{As}_2\text{S}_3$  Chalcogenide glass has been presented based on low-loss Electron Energy Loss Spectroscopy. The results are extendable to the optical regime, based on the small angle scattering approximation. The results allow us to calculate an approximate form of the refractive index, considering constant permeability; and hint the possibility of magnetic alterations induced by electron irradiation.

The calculated results and observations found that high energy electrons induced a reduction in the permittivity, real and imaginary, of  $\text{As}_2\text{S}_3$  thin film. The real permittivity underwent a maximum reduction of  $\sim 40\%$ , while the imaginary permittivity decreased  $\sim 50\%$ . The conspicuous results can be explained in terms of the atomic bond reconfiguration. In this model, the incident electrons break the homopolar and heteropolar bonds, leading to a reduction of the former, *correcting* the *wrong* bonds.

The results are significant to the development of manifold photonic applications, with applications to numerous areas of research and engineering. Namely, the observed reduction in the permittivity could enable a new range of transformation optics devices, which have been so far limited to the realm of far-IR. Furthermore, this results could be capital to future implementation of reconfigurable photonic circuits, infrared telecommunications, photonics crystals, all optical conversion and computing.

- 
- [1] Z. Yang, M. K. Fah, K. A. Reynolds, J. D. Sexton, M. R. Riley, M.-L. Anne, B. Bureau, and P. Lucas, "Opto-electrophoretic detection of bio-molecules using conducting chalcogenide glass sensors," *Optics Express*, vol. 18, p. 26754, Dec. 2010.

- [2] B. J. Eggleton, B. Luther-Davies, and K. Richardson, “Chalcogenide photonics,” *Nature Photonics*, vol. 5, pp. 141–148, 2011.
- [3] M. D. Pelusi, F. Luan, S. J. Madden, D.-y. Choi, D. Bulla, B. Luther-Davies, and B. J. Eggleton, “Chalcogenide Glass Chip Based Nonlinear Signal Processing - OSA Technical Digest (CD),” in *Integrated Photonics Research, Silicon and Nanophotonics*, p. IWC3, Optical Society of America, July 2010.
- [4] B. J. Eggleton, “Chalcogenide photonics: fabrication, devices and applications Introduction,” *Optics Express*, vol. 18, p. 26632, Dec. 2010.
- [5] C. Xiong, L. G. Helt, A. C. Judge, G. D. Marshall, M. J. Steel, J. E. Sipe, and B. J. Eggleton, “Quantum-correlated photon pair generation in chalcogenide As<sub>2</sub>S<sub>3</sub> waveguides,” *Optics Express*, vol. 18, p. 16206, July 2010.
- [6] X. Bendaña, A. Polman, and F. J. García de Abajo, “Single-photon generation by electron beams,” *Nano letters*, vol. 11, pp. 5099–103, Dec. 2011.
- [7] S. Juodkasis, T. Kondo, and H. Misawa, “Three-dimensional recording and structuring of chalcogenide glasses by femtosecond pulses,” in *Proceedings of SPIE*, vol. 5662, pp. 179–184, SPIE, Oct. 2004.
- [8] G. Chen, H. Jain, M. Vlcek, and A. Ganjoo, “Photoinduced volume change in arsenic chalcogenides by bandgap light,” *Phys. Rev. B*, vol. 74, p. 174203, 2006.
- [9] M. I. Kozak, V. Y. Loya, N. P. Golub, and M. Y. Onisâ\texttrademarkko, “Mechanism of photoinduced nanodimensional expansion/contraction in glassy thin layers of As<sub>2</sub>S<sub>3</sub>,” *Theoretical and Experimental Chemistry*, vol. 45, pp. 69–73, May 2009.
- [10] H. Fritzsche and H. Firtzsche, “Photo-induced fluidity of chalcogenide glasses,” *Solid State Communications*, vol. 99, no. 3, p. 153, 1996.
- [11] K. Tanaka, “Photoinduced deformations in chalcogenide glasses: scalar and vectorial,” *Journal of Optoelectronics and Advanced Materials*, vol. 7, no. 5, pp. 2571 – 2580, 2005.
- [12] J. Feinleib, J. P. DeNeufville, S. C. Moss, and S. R. Ovshinsky, “Rapid reversible light-induced crystallization of amorphous semiconductors,” *Applied Physics Letters*, vol. 18, p. 254, Oct. 1971.
- [13] K. Tanaka and K. Shimakawa, “Chalcogenide glasses in Japan: A review on photoinduced phenomena,” *physica status solidi (b)*, vol. 246, pp. 1744–1757, Aug. 2009.
- [14] I. Istvan, *Photo- and ion-induced changes in amorphous chalcogenide films*. PhD thesis, De-

- brecen, 2007.
- [15] J. De Neufville, S. Moss, and S. Ovshinsky, “Photostructural transformations in amorphous As<sub>2</sub>Se<sub>3</sub> and As<sub>2</sub>S<sub>3</sub> films,” *Journal of Non-Crystalline Solids*, vol. 13, no. 2, pp. 191–223, 1974.
  - [16] V. Gopal, “Energy gap-refractive index interrelation,” *Infrared Physics*, vol. 22, no. 5, pp. 255–257, 1982.
  - [17] R. M. Kurtz, W. Lu, J. Piranian, T. Jansson, and A. O. Okorogu, “The Fast Photorefractive Effect and Its Application to Vibrometry,” *Journal of Holography and Speckle*, vol. 5, pp. 149–155, Aug. 2009.
  - [18] V K Tikhomirov and S R Elliott, “The anisotropic photorefractive effect in bulk As<sub>2</sub>S<sub>3</sub> glass induced by polarized subgap laser light,” *Journal of Physics: Condensed Matter*, vol. 7, no. 8, p. 1737, 1995.
  - [19] M. Kowalyshen, *Photoinduced Dichroism in Amorphous As<sub>2</sub>Se<sub>3</sub> Thin Film*. PhD thesis, 2010.
  - [20] V. G. Ta’eed, M. R. E. Lamont, D. J. Moss, B. J. Eggleton, D.-Y. Choi, S. Madden, and B. Luther-Davies, “All optical wavelength conversion via cross phase modulation in chalcogenide glass rib waveguides,” *Optics express*, vol. 14, pp. 11242–7, Nov. 2006.
  - [21] V. Lyubin, M. Klebanov, M. Veinger, I. Lyubina, and B. Sfez, “Photoluminescence and photostructural transformations in neodymium-doped glassy chalcogenide films,” *Optical Materials*, vol. 28, pp. 1115–1117, June 2006.
  - [22] P. Anderson, “Model for the electronic structure of amorphous semiconductors,” *Physical Review Letters*, vol. 34, no. 15, pp. 953–955, 1975.
  - [23] H. Fritzsche, “Toward understanding the photoinduced changes in chalcogenide glasses,” *Semiconductors*, vol. 32, pp. 850–854, Aug. 1998.
  - [24] S. Simdyankin, S. Elliott, Z. Hajnal, T. Niehaus, and T. Frauenheim, “Simulation of physical properties of the chalcogenide glass As<sub>2</sub>S<sub>3</sub> using a density-functional-based tight-binding method,” *Physical Review B*, vol. 69, Apr. 2004.
  - [25] A. Andriesh, M. Iovu, and S. Shutov, *Semiconducting Chalcogenide Glass II - Properties of Chalcogenide Glasses*, vol. 79 of *Semiconductors and Semimetals*. Elsevier, 1st ed., 2004.
  - [26] J. Singh and K. Tanaka, “Photo-structural changes in chalcogenide glasses during illumination,” *Journal of Materials Science: Materials in Electronics*, vol. 18, pp. 423–428, Mar. 2007.
  - [27] T. Suhara, H. Nishihara, and J. Koyama, “Electron-Beam-Induced Refractive-Index Change of Amorphous Semiconductors,” *Japanese Journal of Applied Physics*, vol. 14, pp. 1079–1080,

July 1975.

- [28] N. Nordman and O. Salminen, “Thickness variations in amorphous As<sub>2</sub>S<sub>3</sub> films induced by electron beam,” *Solid State Communications*, vol. 100, pp. 241–244, Oct. 1996.
- [29] N. Nordman and O. Nordman, “Refractive index change caused by electron irradiation in amorphous AsS and AsSe thin films coated with different metals,” *Journal of Applied Physics*, vol. 90, p. 2206, Sept. 2001.
- [30] O. Nordman, N. Nordman, and V. Pashkevich, “Refractive-index change caused by electrons in amorphous AsS and AsSe thin films doped with different metals by photodiffusion,” *Journal of the Optical Society of America B*, vol. 18, p. 1206, Aug. 2001.
- [31] K. Tanaka, “Electron beam induced reliefs in chalcogenide glasses,” *Applied Physics Letters*, vol. 70, p. 261, Jan. 1997.
- [32] J. Perrin, J. Cazaux, and P. Soukiasian, “Optical Constants and Electronic Structure of Crystalline and Amorphous As<sub>2</sub>S<sub>3</sub> in the 3 to 35 eV Range,” *physica status solidi (b)*, vol. 62, pp. 343–350, Apr. 1974.
- [33] R. F. Egerton, *Electron Energy Loss Spectroscopy in the Electron Microscope*. New York: Plenum Press, 2nd ed., 1996.
- [34] R. H. Ritchie, “Plasmon losses by fast electron in thin films,” *Physical Review*, vol. 106, pp. 874–881, 1957.
- [35] P. Nozieres and D. Pines, “Electron interaction in solids: Characteristic energy-loss spectrum,” *Physical Review*, vol. 113, pp. 1254–1267, 1959.
- [36] M. Stöger-Pollach, “Optical properties and bandgaps from low loss EELS: pitfalls and solutions,” *Micron (Oxford, England : 1993)*, vol. 39, pp. 1092–110, Dec. 2008.
- [37] R. F. Egerton, “Electron energy-loss spectroscopy in the TEM,” *Reports on Progress in Physics*, vol. 72, p. 016502, Jan. 2009.
- [38] J. Verbeeck and G. Bertonni, “Deconvolution of core electron energy loss spectra,” *Ultramicroscopy*, vol. 109, pp. 1343–52, Oct. 2009.
- [39] F. J. García de Abajo, “Optical excitations in electron microscopy,” *Reviews of Modern Physics*, vol. 82, pp. 209–275, Feb. 2010.
- [40] L. Zhang, S. Turner, and J. Verbeeck, “Model-based determination of dielectric function by STEM low-loss EELS,” *Physical Review B*, vol. 81, p. 035102, Jan. 2010.
- [41] K. Hoffmann, *Electron Energy Loss Spectroscopy as an Experimental Probe for the Crystal*

*Structure and Electronic Situation of Solids*. Weinheim, Germany: Wiley-VCH Verlag GmbH & Co. KGaA, Apr. 2012.

- [42] J. Ramírez-Malo, E. Márquez, C. Corrales, P. Villares, and R. Jiménez-Garay, “Optical characterization of As<sub>2</sub>S<sub>3</sub> and As<sub>2</sub>Se<sub>3</sub> semiconducting glass films of non-uniform thickness from transmission measurements,” *Materials Science and Engineering: B*, vol. 25, pp. 53–59, June 1994.
- [43] O. Nordman, N. Nordman, and N. Peyghambarian, “Electron beam induced changes in the refractive index and film thickness of amorphous As<sub>x</sub>S<sub>100-x</sub> and As<sub>x</sub>Se<sub>100-x</sub> films,” *Journal of Applied Physics*, vol. 84, p. 6055, Dec. 1998.
- [44] A. Kovalskiy, J. Neilson, A. Miller, F. Miller, M. Vlcek, and H. Jain, “Comparative study of electron- and photo-induced structural transformations on the surface of As<sub>35</sub>S<sub>65</sub> amorphous thin films,” *Thin Solid Films*, vol. 516, pp. 7511–7518, Sept. 2008.
- [45] a. M. Nastas, a. M. Andriesh, V. V. Bivol, a. M. Prisakar, and G. M. Tridukh, “Effect of electric field on photoinduced changes in the optical properties of chalcogenide glassy semiconductors,” *Technical Physics Letters*, vol. 32, pp. 45–47, Jan. 2006.
- [46] V. Arkhipov, M. Iovu, M. Iovu, A. Rudenko, and S. Shutov, “Negative transient currents in amorphous semiconductors,” *International Journal of Electronics*, vol. 51, pp. 735–742, 1981.
- [47] K. Tanaka, “Chemical and medium-range orders in As<sub>2</sub>S<sub>3</sub> glass,” *Physical Review B*, vol. 36, no. 18, pp. 9746–9752, 1987.
- [48] J. M. Lee, G. Pfeiffer, M. A. Paesler, D. E. Sayers, and A. Fontaine, “Photon intensity-dependent darkening kinetics in optical and structural anisotropy in a-As<sub>2</sub>S<sub>3</sub>: A study of X-ray absorption spectroscopy,” *Journal of Non-Crystalline Solids*, vol. 114, pp. 52–54, 1989.
- [49] H. Nishihara, Y. Handa, T. Suhara, and J. Koyama, “Direct writing of optical gratings using a scanning electron microscope,” *Applied Optics*, vol. 17, p. 2342, Aug. 1978.